The Journal of Fourier Analysis and Applications

Volume 8, Issue 5, 2002

Microlocal Analysis of an FBP Algorithm for Truncated Spiral Cone Beam Data

Alexander Katsevich

Communicated by Eric Quinto

ABSTRACT. In this article we propose an FBP-type algorithm for inversion of spiral cone beam data, study its theoretical properties, and illustrate performance of the algorithm by numerical examples. In particular, it is shown that the algorithm does not reconstruct f exactly, but computes the result of applying a pseudo-differential operator (PDO) with singular symbol to f. Away from critical directions the amplitude of this PDO is homogeneous of order zero in the dual variable, bounded, and approaches one as the pitch of the spiral goes to zero. Numerical experiments presented in the article show that even when the pitch is relatively large, the accuracy of reconstruction is quite high. On the other hand, under certain circumstances, the algorithm produces artifacts typical of all FBP-type algorithms.

1. Introduction

Spiral computed tomography (CT) involves continuous data acquisition throughout the volume of interest by simultaneously moving the patient through the gantry while the x-ray source rotates. Spiral CT has numerous advantages over conventional CT and is now a standard medical imaging modality. There is, however, one major difficulty in image reconstruction from the spiral CT data. The problem is that each slice is illuminated from only one direction and, therefore, there is not enough data for exact slice-by-slice reconstruction if the detector array is one-dimensional. A way around this is to find the missing data approximately by interpolating the projection data corresponding to nearby

Math Subject Classifications. 44A12, 65R10, 92C55.
Keywords and Phrases. cone-beam, spiral tomography, approximate reconstruction, filtered back-projection algorithm, analysis of artifacts.
Acknowledgements and Notes. This research was supported in part by NSF grant DMS-9704285.

ISSN 1069-5869

sections. Unfortunately, interpolation leads to artifacts. Also, reformatted (coronal/sagittal) spiral CT images have limited axial resolution. It appears that future developments of spiral CT will involve using two-dimensional (2-D) multirow detectors instead of one-dimensional single row ones. This will help to further reduce artifacts, increase patient throughput, and improve spatial resolution of coronal/sagittal reconstructions.

In most cases the axial length of the detector will be too small compared with the object size, and cone beam projections will be truncated. Several approaches for handling truncated cone beam projections have been proposed. They can be classified into two groups: theoretically exact and approximate. Most of exact algorithms are based on computing the Radon transform for a given plane by partitioning the plane in a manner determined by the spiral path of the x-ray source [17, 18, 11]. Even though exact algorithms are more accurate, they are computationally very intensive. Approximate algorithms are much more efficient (see e. g., [9, 14, 2] for some most recent techniques), but produce artifacts. Frequently, the consequences of introducing approximation are not theoretically analyzed and the insight into the nature of artifacts is gained from numerical experiments. A very popular class of approximate algorithms is based on various modifications of the Feldkamp, Davis, Kress algorithm [4]. They all are of the filtered backprojection (FBP) type and, therefore, quite efficient (see [10] for the analysis of performance of two such algorithms). In this article we propose another FBP algorithm, derive its theoretical properties, discuss the nature of artifacts, and illustrate performance of the algorithm by numerical examples.

An alternative approach to image reconstruction from cone beam data that can also be used in the case of axially truncated projections is local tomography (see [13, 6]). The idea of the method is to reconstruct, instead of the original image f, the result of applying a pseudo-differential operator (PDO) of positive order (most frequently of order one) to f, thus, emphasizing discontinuities in f. In a very general setting theoretical foundation of 3-D local tomography is contained in [5]. Further details are worked out in [15, 6, 12]. As opposed to 2-D local tomography (see e. g., [16, 3]), in the 3-D case the corresponding PDO has singular symbol. For example, as follows from Proposition 3.2 in [6] and a similar result in [12], this symbol is unbounded in a neighborhood of certain critical directions. The algorithm proposed in this article also does not reconstruct f exactly, but computes the result of applying a PDO to f. In contrast to local tomography, the amplitude of this PDO is homogeneous of order zero and uniformly bounded away from critical directions. Moreover, the amplitude approaches one as the pitch of the spiral goes to zero. Numerical experiments presented in the article show that even when the pitch is relatively large, the accuracy of reconstruction is quite high. On the other hand, under certain circumstances, the algorithm produces artifacts typical of all FBP-type algorithms.

The article is organized as follows. In Section 2 we show that the function being computed is the result of applying a PDO $\mathcal{B}$ with singular symbol to the original image $f \in C_0^\infty$. We find explicitly not just the principal symbol of $\mathcal{B}$, but the complete symbol (or, amplitude) of $\mathcal{B}$. In principle, this can allow one to go beyond the microlocal analysis of $\mathcal{B}f$ and study a wide variety of problems, such as estimation of $f - \mathcal{B}f$ in some norm, estimation of discretization errors, etc. A formal derivation of the amplitude, which illustrates the main idea of the proof, is also in Section 2. The remainder of the proof, which is technical and could have obscured the main idea, is contained in Sections 5 and 6. In Section 3 we show that $\mathcal{B}$ can be extended to act on distributions and prove that away from certain critical directions $\mathcal{B}$ behaves just like an ordinary PDO. Results of numerical experiments on simulated data are presented in Section 4.

2. Analysis of the Algorithm. Part 1

First we introduce the necessary notation. Let

$$\begin{aligned} C_h &:= \left\{ y \in \mathbb{R}^3 : \; y_1 = R\cos(2\pi s),\, y_2 = R\sin(2\pi s),\, y_3 = sh,\, s \in I_h \right\} , \\ I_h &:= [a/h,\, b/h] , \end{aligned} \tag{2.1}$$

where $h > 0$, $b > a$, be a spiral, and U be an open set strictly inside the spiral:

$$\overline{U} \subset \left\{ x \in \mathbb{R}^3 : \; x_1^2 + x_2^2 < r^2,\, a < x_3 < b \right\},\; 0 < r < R \, . \tag{2.2}$$

S^2 is the unit sphere in $\mathbb{R}^3$, and

$$D_f(y,\beta) := \int_0^\infty f(y+\beta t)\, dt, \;\; \beta \in S^2 \, ; \tag{2.3}$$

$$\beta(s,x) := \frac{x - y(s)}{|x - y(s)|}, x \in U, s \in I_h; \;\; \Pi(x,\xi) := \left\{ y \in \mathbb{R}^3 : \; (y-x)\cdot\xi = 0 \right\} \; ; \tag{2.4}$$

that is $D_f(y,\beta)$ is the cone-beam transform of f. Given $(x,\xi) \in U \times (\mathbb{R}^3 \setminus 0)$, let $s_j = s_j(\xi, \xi\cdot x)$, $j = 1, 2, \ldots$, denote finitely many points of intersection of the plane $\Pi(x,\xi)$ with C_h. Also, $\dot{y}(s) := dy/ds$, e_3 is the unit vector along the axis of the spiral, and for vectors $x, y, \xi \in \mathbb{R}^3$ the subscript '3' denotes their component along e_3.

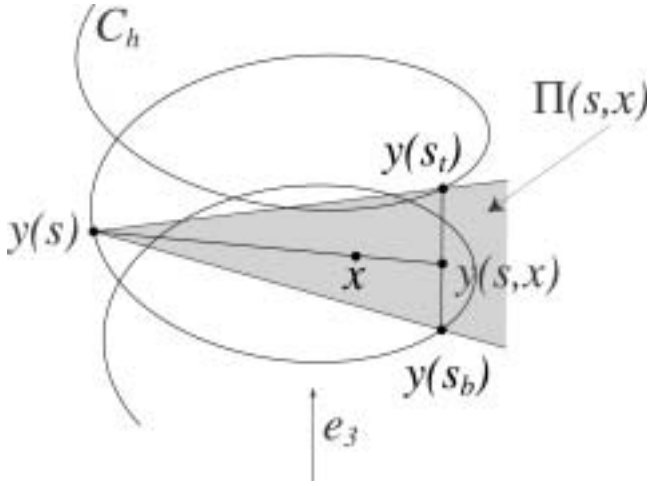

FIGURE 1 Illustration of the construction of $\phi(s,x)$.

As is well known, the smallest detector array required for exact reconstruction of f is obtained from the requirement that all rays diverging from the source, traversing the object, and located between the upper and lower turns of the spiral be measured [18, 1, 9]. In view of this, we construct the following cut-off/weighting function ϕ. Given $y(s) \in C_h$ and $x \in U$, let $\Pi(s,x)$ be the plane through $y(s)$, x, and parallel to e_3 (see Figure 1). Let $y(s_{b,t}) \in C_h \cap \Pi(s,x)$, $s_{b,t} = s_{b,t}(s,x)$, be two points located immediately above and below $y(s)$ on the opposite side of the spiral. Obviously, $y_3(s_b) < y_3(s) < y_3(s_t)$ and

$y_3(s_t) - y_3(s_b) = h$. Further, let $y(s,x)$ be the point of intersection of the line through $y(s)$, x and the line through $y(s_b)$, $y(s_t)$. Then,

$$\phi(s,x) := \frac{\chi(s,x)}{\sum_{y(s_l)\in C_h\cap\Pi(s,x)}\chi(s_l,x)}\,, \tag{2.5}$$

$$\chi(s,x) := \chi_0\left(\frac{y_3(s,x) - 0.5[y_3(s_b)+y_3(s_t)]}{h}\right)\,, \tag{2.6}$$

where $\chi_0 \in C_0^\infty(\mathbb{R})$ is a fixed function with the property:

$$\chi_0(t) = \begin{cases} 1, & |t| \le 0.5\,, \\ 0, & |t| \ge 0.5+\epsilon\,, \end{cases} \quad \epsilon > 0\,. \tag{2.7}$$

It is important to stress that $s_{b,t}$ in the definition of $\chi(s,x)$ depend on s. Thus, $s_{b,t} = s_{b,t}(s,x)$ that have been implicitly used in the numerator in (2.5) are, in general, different from $s_{b,t} = s_{b,t}(s_l,x)$ that have been implicitly used in the denominator. Clearly, $0 \le \phi(s,x) \le 1$, and

$$\sum_{y(s)\in C_h\cap\Pi(x)} \phi(s,x) = 1,\ x\in U\,, \tag{2.8}$$

for any plane $\Pi(x)$ containing x and parallel to e_3.

The role of $\phi(s,x)$ is two-fold. First, it localizes the approximate inversion formula in the axial direction. As is seen from Figure 1, if the source $y(s)$ moves up (or, down) along the spiral, the point $y(s,x)$ moves down (or, up) along the segment $[y(s_b), y(s_t)]$. When $y(s,x)$ falls outside a neighborhood of the segment, $\phi(s,x)$ vanishes. The second role is that $\phi(s,x)$ deals with redundancy in the data and averages multiple contributions from various cone-beam projections to the same pixels in the reconstructed image. This averaging, however, is not very apparent, because it takes place at the microlocal level. As follows from (2.8), for directions perpendicular to the axis of the spiral the weights in front of contributions from multiple projections add up exactly to one.

Using (2.5) denote

$$\begin{aligned} e(s,x) &:= \frac{[\beta(s,x)\times\dot y(s)]\times\beta(s,x)}{|[\beta(s,x)\times\dot y(s)]\times\beta(s,x)|},\ \psi_1(s,x) := \phi(s,x)\frac{e(s,x)\cdot\dot y(s)}{|x-y(s)|^2}\,, \\ \psi_2(s,x) &:= \frac{\phi_s'(s,x)}{|x-y(s)|} + \phi(s,x)\frac{\beta(s,x)\cdot\dot y(s)}{|x-y(s)|^2}\,. \end{aligned} \tag{2.9}$$

Clearly, $e(s,x)$ is a unit vector in the plane spanned by $\beta(s,x)$ and $\dot y(s)$ and perpendicular to $\beta(s,x)$. For $f\in C_0^\infty(U)$ define

$$\begin{aligned} (\mathcal{B}f)(x) :=& \\ &-\frac{1}{2\pi^2}\int_{I_h}\psi_1(s,x)\int_0^{2\pi} D_f(y(s),\cos\gamma\beta(s,x) \quad + \sin\gamma e(s,x))\frac{\cos\gamma}{\sin^2\gamma}\,d\gamma\,ds \\ &+\frac{1}{2\pi^2}\int_{I_h}\psi_2(s,x)\int_0^{2\pi} D_f(y(s),\cos\gamma\beta(s,x)+\sin\gamma e(s,x))\frac{1}{\sin\gamma}\,d\gamma\,ds\,. \end{aligned} \tag{2.10}$$

The first term of (2.10) is related to a Feldkamp-like algorithm discussed in [19]. In both algorithms redundancy in the data is handled using the ideas based on the PI window. One

of the differences is that 1-D ramp filtering is used in [19], while in (2.10) the convolution is on the unit circle with a ramp-like filter $\cos\gamma/\sin^2\gamma$. The second term in (2.10) is added to improve the overall accuracy of the reconstruction formula. This term can be derived using the ideas of [7].

Our first result is the following theorem.

Theorem 1.

The operator $\mathcal{B}$ can be written in the form

$$(\mathcal{B}f)(x) = \frac{1}{(2\pi)^3}\int_{\mathbb{R}^3} B(x,\xi)\tilde{f}(\xi)e^{-i\xi\cdot x}\,d\xi + \frac{2i}{(2\pi)^3}\int_{I_h}\frac{\phi(s,x)}{|x-y(s)|}\int_{\substack{\xi=r[\beta\times e]\\ -\infty<r<\infty}}\tilde{f}(\xi)\left(\xi\cdot e_s'(s,x)\right)e^{-i\xi\cdot x}\,dr\,ds\,, \tag{2.11}$$

where

$$B(x,\xi) = \sum_j \phi(s_j(\xi,\xi\cdot x),x),\ (x,\xi)\in U\times\left(\mathbb{R}^3\setminus 0\right)\,. \tag{2.12}$$

Moreover,

$$B(x,\xi) = 1,\ \xi_3 = 0, x\in U\,, \tag{2.13}$$

and for every $\delta>0$ one has

$$B(x,\xi) = 1+O(h),\ x\in U, |\xi_3|/|\xi|<1-\delta,\ h\to 0\,. \tag{2.14}$$

Several remarks about the properties of $\mathcal{B}$ are in order.

(1) It follows from (2.5)–(2.7) and (2.9), (2.10) that reconstruction of a given slice $x_3 = x_3^{(0)}$ of $\mathcal{B}f$ only requires cone beam projections to be known in a region $s\in[(x_3^{(0)}/h) - \Delta s, (x_3^{(0)}/h)+\Delta s]$, where Δs is independent of the axial extent of supp f and is bounded as $h\to 0$. Thus, reconstruction formula (2.10) solves the so-called long object problem ([2], Definition 1). It is easy to see that if $y(s,x)$ coincides with either $y(s_b)$ or $y(s_t)$, then, the segment $[y(s), y(s,x)]$ is precisely the PI line containing x (see [2], Definition 3). In view of the discussion following (2.8), in the limit $\epsilon\to 0$ the algorithm requires the theoretically minimal segment of the spiral.

(2) If we think of vectors β, e, and $\dot{y}$ as being attached to $y(s)$, then, all vectors $\cos\gamma\beta+\sin\gamma e$ in (2.10) belong to the plane spanned by β and $\dot{y}$. Therefore, the preceding remark implies that the required axial extent of the detector is $O(h)$.

(3) Suppose f is independent of x_3 in a sufficiently large $O(h)$-size neighborhood of $x_3 = x_3^{(0)}$. As follows from remark (1), $(\mathcal{B}f)(x_1,x_2,x_3^{(0)}) = (\mathcal{B}g)(x_1,x_2,x_3^{(0)})$, where g is independent of x_3: $g(x) := f(x_1,x_2,x_3^{(0)})$. Clearly,

$$\tilde{g}(\xi) = 2\pi\delta(\xi_3)\iint f\left(x_1,x_2,x_3^{(0)}\right)e^{i(\xi_1x_1+\xi_2x_2)}\,dx_1\,dx_2\,. \tag{2.15}$$

Replacing $\tilde{f}$ with $\tilde{g}$ in (2.11), using (2.13), and the property

$$\inf_{\substack{s\in I_h, x\in U\\ \phi(s,x)>0}}|e_3\cdot[\beta(s,x)\times e(s,x)]|>0\,, \tag{2.16}$$

we obtain that the first term on the right in (2.11) gives $f(x_1, x_2, x_3^{(0)})$, and the second term—zero. Thus, the slice $x_3 = x_3^{(0)}$ of f will be reconstructed theoretically exactly.

(4) Property (2.14) implies that $B(x, \xi) \to 1, h \to 0$, pointwise for all $\xi, \xi_3/|\xi| \neq \pm 1$. Moreover, (2.5)–(2.7) and (2.9), (2.10) imply that $[\beta(s, x) \times e(s, x)] \cdot e_s'(s, x) = O(h)$ on supp $\phi(s, x)$, and the second term on the right in (2.11) goes to zero as $h \to 0$. Thus, in some sense, $\mathcal{B}$ approaches the identity operator as $h \to 0$.

(5) For finite $h > 0$ the operator $\mathcal{B}$ is not a PDO in the classical sense, because its symbol is singular. Introduce the following critical set

$$\text{Crit}(C_h, \phi) := \left\{(x, \xi) \in U \times \left(\mathbb{R}^3 \setminus 0\right) : y(s) \in \Pi(x, \xi), \xi \cdot \dot{y}(s) = 0, s \in I_h(x)\right\}, \quad (2.17)$$

where

$$I_h(x) := \overline{\{s \in I_h : \phi(s, x) > 0\}}, \quad (2.18)$$

and the overbar denotes closure. Basically, $\text{Crit}(C_h, \phi)$ consists of all $(x, \xi) \in U \times (\mathbb{R}^3 \setminus 0)$ such that $\Pi(x, \xi)$ is tangent to C_h at some $y(s), s \in I_h(x)$. As follows from (2.12), singsupp $B \subset \text{Crit}(C_h, \phi)$. In addition, the second term on the right in (2.11) can be regarded as a distribution acting on $\tilde{f}$, depending on x as a parameter, and with support contained in $\text{Crit}(C_h, \phi)$. However, $\mathcal{B}$ behaves just like a conventional PDO outside $\text{Crit}(C_h, \phi)$ (see Theorem 5 below). In particular, if f is a distribution (see Theorem 2 below), then, most of the wave front set of f: $\{(x, \xi) \in WF(f) : (x, \xi) \notin \text{Crit}(C_h, \phi)\}$ will be reconstructed without artifacts. Nonsmoothness of the symbol of $\mathcal{B}$ will lead to artifacts. Thus, in general, $WF(\mathcal{B}f) \not\subset WF(f)$.

(6) By construction, the number of nonzero terms in (2.12) is uniformly bounded. Therefore, $B(x, \xi)$ is uniformly bounded on $(U \times (\mathbb{R}^3 \setminus 0)) \setminus \text{Crit}(C_h, \phi)$.

Proof of Theorem 1. Using (2.3), consider the first integral with respect to γ in (2.10):

$$\begin{aligned}
&\int_0^{2\pi} \int_0^{\infty} f(y(s) + t(\cos\gamma\beta(s, x) + \sin\gamma e(s, x))) \frac{t\cos\gamma}{t^2\sin^2\gamma} t\, dt\, d\gamma \\
&= \int_{\mathbb{R}^2} f(y(s) + u) \frac{u \cdot \beta(s, x)}{(u \cdot e(s, x))^2}\, du \\
&= \frac{1}{8\pi^3} \int_{\mathbb{R}^3} \tilde{f}(\xi) \int_{\mathbb{R}^2} e^{-i\xi\cdot(y(s)+u)} \frac{u \cdot \beta(s, x)}{(u \cdot e(s, x))^2}\, du\, d\xi \\
&= \frac{1}{8\pi^3} \int_{\mathbb{R}^3} \tilde{f}(\xi) e^{-i\xi\cdot y(s)} \left[\int_{\mathbb{R}} e^{-i\xi_1 u_1} u_1\, du_1 \int_{\mathbb{R}} e^{-i\xi_2 u_2} \frac{du_2}{u_2^2}\right] d\xi \\
&= \frac{1}{8\pi^3} \int_{\mathbb{R}^3} \tilde{f}(\xi) e^{-i\xi\cdot y(s)} 2\pi i \delta'(\xi_1)(-\pi|\xi_2|)\, d\xi \\
&= \frac{-i}{4\pi} \int_{\mathbb{R}^3} \tilde{f}(\xi) e^{-i\xi\cdot y(s)} \delta'(\xi \cdot \beta(s, x))|\xi \cdot e(s, x)|\, d\xi\,,
\end{aligned} \quad (2.19)$$

where du is the Lebesgue measure on the plane through the origin and parallel to $\beta(s, x)$, $e(s, x)$. In (2.19) we have assumed without loss of generality that the ξ_1-axis is parallel to $\beta(s, x)$, and the ξ_2-axis is parallel to $e(s, x)$. Since derivation (2.19) is central in the proof of the main result, regularization of the divergent integrals of (2.19) is discussed in Section 5 below. Substituting the part of the integrand in (2.19) that depends on s into (2.10), assuming

$\xi \cdot \dot{y}(s) \neq 0$ (in a neighborhood of all points $y(s_j)$, $s_j = s_j(\xi, \xi \cdot x)$, where $\phi(s_j, x) \neq 0$), and changing variables $s \to t = \xi \cdot y(s)$, we find

$$\begin{aligned}
&\int_{I_h} \phi(s,x) \frac{|e(s,x)\cdot \dot{y}(s)|}{|x-y(s)|^2} e^{-i\xi\cdot y(s)} \delta'\left(\xi \cdot \frac{x-y(s)}{|x-y(s)|}\right) |\xi \cdot e(s,x)|\, ds \\
&\quad = \int_{I_h} \phi(s,x) |e(s,x)\cdot \dot{y}(s)| e^{-i\xi\cdot y(s)} \delta'(\xi\cdot(x-y(s)))|\xi\cdot e(s,x)|\, ds \\
&\quad = \int_{-\infty}^{\infty} \phi(s,x) A(\xi,s,x) e^{-it} \delta'(\xi\cdot x - t)\, dt \\
&\quad = \left[-i \sum_j \phi(s_j,x) A(\xi,s_j,x) + \sum_j \frac{1}{t_s'} \frac{\partial}{\partial s} \{\phi(s,x)A(\xi,s,x)\}\Big|_{s=s_j} \right] e^{-i\xi\cdot x} ,
\end{aligned} \tag{2.20}$$

where we have denoted

$$A(\xi,s,x) := \frac{|e(s,x)\cdot\dot{y}(s)|\,|\xi\cdot e(s,x)|}{|\xi\cdot\dot{y}(s)|} . \tag{2.21}$$

It is interesting to note that even though the factor $1/|x-y(s)|$ inside δ' in the first line in (2.20) depends on the variable of integration s, calculation shows that since this factor does not vanish one can move it outside δ' using the homogeneity property of δ' as if it were a constant. Further, our assumptions imply $e(s_j,x)\cdot\dot{y}(s_j) > 0, x \in U$. By a simple geometrical argument,

$$A(\xi,s_j,x) \equiv 1 \text{ if } \xi\cdot\dot{y}(s_j) \neq 0 . \tag{2.22}$$

Obviously, $t_s'(s_j) = \xi\cdot\dot{y}(s_j)$. Further, by (2.22),

$$\frac{\partial}{\partial s}\{\phi(s,x)A(\xi,s,x)\}\Big|_{s=s_j} = \phi_s'(s_j,x) + \phi(s_j,x)A_s'(\xi,s_j,x) . \tag{2.23}$$

By construction (omitting, for convenience, the arguments s and x),

$$e = a\beta + b\dot{y},\ e\cdot\beta = 0,\ e\cdot e = 1,\ b > 0 , \tag{2.24}$$

for some scalar functions $a = a(s,x)$ and $b = b(s,x)$. This implies

$$e = b[\dot{y} - (\beta\cdot\dot{y})\beta],\ b^2\left[(\dot{y}\cdot\dot{y}) - (\beta\cdot\dot{y})^2\right] = 1 . \tag{2.25}$$

Hence,

$$\begin{aligned}
A(\xi,s,x) &= b^2 \frac{\left[(\dot{y}\cdot\dot{y}) - (\dot{y}\cdot\beta)^2\right]|(\xi\cdot\dot{y}) - (\beta\cdot\dot{y})(\xi\cdot\beta)|}{|\xi\cdot\dot{y}|} \\
&= 1 - (\beta\cdot\dot{y})\frac{\xi\cdot\beta}{\xi\cdot\dot{y}} = 1 + \frac{\beta\cdot\dot{y}}{|x-y(s)|}\frac{\xi\cdot(y(s)-x)}{\xi\cdot\dot{y}} ,
\end{aligned} \tag{2.26}$$

where we have assumed that s is sufficiently close to s_j and $\xi\cdot\beta$ is close to zero (recall that s_j's are found by solving $(x-y(s))\cdot\xi = 0$). Differentiation of (2.26) yields

$$A_s'(\xi,s_j,x) = \frac{\beta(s_j,x)\cdot\dot{y}(s_j)}{|x-y(s_j)|},\ \xi\cdot\dot{y}(s_j) \neq 0 . \tag{2.27}$$

Thus, using (2.19)–(2.23) and (2.27) we obtain the following (formal) expression for the first integral in (2.10):

$$I_1(x) = \frac{1}{(2\pi)^3}\int_{\mathbb{R}^3} \tilde{f}(\xi)e^{-i\xi\cdot x} \times \sum_j \left\{ \phi(s_j,x) + i\frac{\phi_s'(s_j,x)+\phi(s_j,x)(\beta(s_j,x)\cdot\dot{y}(s_j))|x-y(s_j)|^{-1}}{\xi\cdot\dot{y}(s_j)} \right\} d\xi \ , \quad (2.28)$$
$$s_j = s_j(\xi, \xi\cdot x) \ .$$

Consider now the second integral in (2.10). Similarly to (2.19),

$$\int_0^{2\pi}\int_0^{\infty} f(y(s)+t(\cos\gamma\beta(s,x)+\sin\gamma e(s,x)))\frac{t\,dt}{t\sin\gamma}\,d\gamma = \frac{-i}{4\pi}\int_{\mathbb{R}^3}\tilde{f}(\xi)e^{-i\xi\cdot y(s)}\delta(\xi\cdot\beta(s,x))\,\mathrm{sgn}(\xi\cdot e(s,x))\,d\xi \ . \quad (2.29)$$

Similarly to (2.20), we find formally

$$I_2(x) = -\frac{i}{(2\pi)^3}\int_{\mathbb{R}^3}\tilde{f}(\xi)e^{-i\xi\cdot x} \times \sum_j \left\{\phi_s'(s_j,x)+\phi(s_j,x)(\beta\cdot\dot{y}(s_j))|x-y(s_j)|^{-1}\right\}\frac{\mathrm{sgn}(\xi\cdot e(s_j,x))}{|\xi\cdot\dot{y}(s_j)|}\,d\xi \ , \quad (2.30)$$
$$s_j = s_j(\xi,\xi\cdot x) \ .$$

Since s_j's are found solving $\xi\cdot\beta(s,x)=0$, we have from (2.24), (2.25): $\xi\cdot e(s,x) = b(\xi\cdot\dot{y}(s_j))$, where $b>0$, that is

$$\mathrm{sgn}(\xi\cdot e(s_j,x)) = \mathrm{sgn}(\xi\cdot\dot{y}(s_j)), \ \frac{\mathrm{sgn}(\xi\cdot e(s_j,x))}{|\xi\cdot\dot{y}(s_j)|} = \frac{1}{\xi\cdot\dot{y}(s_j)} \ . \quad (2.31)$$

Combining (2.28), (2.30), and (2.31) formally gives the first term on the right in (2.11), where $B(x,\xi)$ is as in (2.12). The reasons why our proof is only formal at this point and the second term on the right in (2.11) has been lost are as follows: (1) directions $\{\xi\in S^2 : \xi\cdot\dot{y}(s_j)=0\}$ have been ignored; and (2) the step from (2.19) to (2.20) which involves changing the order of integration have not been justified. See Section 6 at the end of the article for the remainder of the proof.

Property (2.13) follows immediately from (2.8) and (2.12). To prove (2.14) fix $(x,\xi)\in U\times S^2, |\xi_3|\neq 1$, and suppose without loss of generality that $x_3=0$. Let θ be the polar angle in the plane through x and perpendicular to $\alpha := (\xi\times e_3)/|\xi\times e_3|$, and $\Theta(\theta)$ be the corresponding unit vector. Replace ξ with $\Theta(\theta)$ in (2.12):

$$B(x,\Theta) = \sum_j \phi(s_j(\Theta,\Theta\cdot x),x), \ \Theta=\Theta(\theta) \ , \quad (2.32)$$

and let $\Theta(\theta)$ rotate from the initial position along ξ until Θ becomes horizontal, i. e., $\Theta\cdot e_3 = 0$. Clearly we can choose this rotation so that Θ is never vertical. By construction, the number of nonzero terms in the sum in (2.32) is uniformly bounded as $h\to 0$ and Θ rotates. Consider one such term. One has

$$\frac{\partial}{\partial\theta}\phi(s_j(\Theta,\Theta\cdot x),x) = \phi_s'(s_j,x)\frac{\partial s_j}{\partial\theta} \ . \quad (2.33)$$

Simple calculation based upon the discussion preceding (2.5) shows that the numerator in (2.5) can be written as

$$\chi(s,x) = \chi_0\left(s(1-\kappa) - \frac{s_b+s_t}{2}\right),$$
$$\kappa = \sqrt{\frac{(y_1(s_b)-y_1(s))^2+(y_2(s_b)-y_2(s))^2}{(x_1-y_1(s))^2+(x_2-y_2(s))^2}}\,. \tag{2.34}$$

Recall that s_l [see the denominator in (2.5)] and s_b, s_t among them are determined by finding points of intersection of the vertical plane through $y(s)$ and x with C_h. Thus, the intersection is always transversal and $\partial s_l/\partial s$ is bounded as $h \to 0$. For the same reason, $\partial s_{b,t}/\partial s_l$ are bounded, cf. the remark following (2.7). This also implies that $\partial\kappa/\partial s$ is bounded as $h \to 0$. As follows from the discussion preceding (2.5) and (2.6), (2.7)

$$\inf_{\substack{x\in U, s\in I_h,\\ h\to 0}} \sum_{y(s_l)\in C_h\cap\Pi(s,x)} \chi(s_l,x) = 1\,, \tag{2.35}$$

and the number of nonzero terms in (2.35) is uniformly bounded. Thus, our argument implies that $\phi_s'(s_j,x)$ is bounded as $h \to 0$. By construction, s_j's in (2.32) are found by solving

$$(x-y(s))\cdot\Theta(\theta) = 0,\ \Theta(\theta)\cdot\alpha = 0\,. \tag{2.36}$$

Differentiating (2.36) with respect to θ, we find

$$\frac{\partial s_j}{\partial\theta} = \pm\frac{(x-y(s_j))\cdot\Theta^\perp}{\dot y(s_j)\cdot\Theta},\ \Theta^\perp = \Theta\times\alpha\,. \tag{2.37}$$

where '+' or '−' is chosen depending upon the direction of rotation of $\Theta(\theta)$. By construction [cf. (2.6)], all the nonzero terms in (2.32) satisfy

$$(x-y(s_j))\cdot e_3 = O(h) \text{ and } \dot y(s_j)\cdot\Theta \neq 0 \tag{2.38}$$

for h small enough. Since $\Theta(\theta)$ is never parallel to e_3, we have

$$\xi = a_1(\theta)\Theta(\theta) + b_1(\theta)e_3 \tag{2.39}$$

for some bounded $a_1(\theta)$, $b_1(\theta)$, and, therefore, $(x-y(s_j))\cdot\xi = O(h)$. Thus,

$$x - y(s_j) = a_2\alpha + b_2\xi + c_2e_3,\ b_2, c_2 = O(h)\,, \tag{2.40}$$

and $\alpha\times(x-y(s_j)) = O(h)$. Using (2.37) we have:

$$(x-y(s_j))\cdot\Theta^\perp = (x-y(s_j))\cdot[\Theta\times\alpha] = \Theta\cdot[\alpha\times(x-y(s_j))] = O(h)\,. \tag{2.41}$$

From (2.33) and (2.37):

$$\frac{\partial}{\partial\theta}B(x,\Theta(\theta)) = O(h),\ h\to 0\,, \tag{2.42}$$

that is $B(x,\Theta(\theta))$ can only change by $O(h)$ when $\Theta(\theta)$ rotates according to our assumptions. Combining with (2.13) proves (2.14). □

3. Action of $\mathcal{B}$ on Distributions

In what follows h will be assumed constant and omitted from notation.

Theorem 2.

The operator $\mathcal{B}$ extends to a continuous map $\mathcal{B}: \mathcal{E}'(U) \to \mathcal{D}'(U)$.

Proof. We need to show that the dual operator $\mathcal{B}^*: C_0^\infty(U) \to C^\infty(U)$ is continuous. To find $\mathcal{B}^*$, rewrite $\mathcal{B}f$ as follows [cf. (2.19)]:

$$\begin{aligned}(\mathcal{B}f)(x) = -\frac{1}{2\pi^2}\int_I\int_{\mathbb{R}^2} &\frac{\psi_1(s,x)u_1 - \psi_2(s,x)u_2}{u_2^2} \\ &\times f(y(s) + u_1\beta(s,x) + u_2 e(s,x))\,du_1\,du_2\,ds\ .\end{aligned} \tag{3.1}$$

By construction,

$$e(s,x) = a(s,x)\frac{x - y(s)}{|x - y(s)|} + b(s,x)\dot{y}(s)\ , \tag{3.2}$$

where a, b are smooth and $\inf_{x\in U, s\in I(x)} b(s,x) > 0$. Changing variables in (3.1):

$$v_1 = \frac{u_1 + au_2}{|x - y(s)|},\ v_2 = bu_2\ , \tag{3.3}$$

we get

$$\begin{aligned}(\mathcal{B}f)(x) &= \int_I\int_{\mathbb{R}^2} \frac{A(s,x,v_1,v_2)}{v_2^2} f(y(s) + v_1(x - y(s)) + v_2\dot{y}(s))\,dv_1\,dv_2\,ds\ , \\ A(s,x,v_1,v_2) &= -\frac{b}{2\pi^2}\left\{\psi_1\left(v_1|x - y(s)| - a\frac{v_2}{b}\right) - \psi_2\frac{v_2}{b}\right\}|x - y(s)|\chi(v_1,v_2)\ ,\end{aligned} \tag{3.4}$$

where $\chi \in C_0^\infty(\mathbb{R}^2)$,

$$\chi(v_1,v_2) \equiv 1 \text{ if } y(s) + v_1(x - y(s)) + v_2\dot{y}(s) \in U \tag{3.5}$$

for some $x \in U$ and $s \in I(x)$. Since U is strictly inside the spiral, we can assume that $v_1 > 0$ is bounded away from zero on supp χ. Fix $g \in C_0^\infty(U)$, then, (3.4) implies after a change of variables

$$\begin{aligned}(\mathcal{B}f, g) &= \int_{\mathbb{R}^3} f(y)\left\{\int_I\int_{\mathbb{R}^2} \frac{A(s,x(\cdot),v_1,v_2)}{v_1^3 v_2^2} g(x(\cdot))\,dv_1\,dv_2\,ds\right\}dy\ , \\ x(\cdot) &:= v_1^{-1}(y - y(s) - v_2\dot{y}(s)) + y(s)\ .\end{aligned} \tag{3.6}$$

Thus,

$$\left(\mathcal{B}^*g\right)(y) = \int_I\int_{\mathbb{R}^2} \frac{A(s,x(\cdot),v_1,v_2)}{v_1^3 v_2^2} g(x(\cdot))\,dv_1\,dv_2\,ds\ . \tag{3.7}$$

Since $v_1 > 0$ is bounded away from zero in (3.7) and $1/v_2^2$ is a well-defined distribution acting on a C_0^∞ function, it is obvious that $\mathcal{B}^*: C_0^\infty(U) \to C^\infty(U)$ is continuous. The desired assertion follows from duality. □

Theorem 3.

Let $V \times \Omega$, $\overline{V} \subset U$, $\Omega \subset \mathbb{R}^3 \setminus 0$, be an open conic set and $\overline{(V \times \Omega)} \cap \mathrm{Crit}(I, \phi) = \varnothing$. Let $f \in \mathcal{E}'(U)$ satisfy $WF(f) \subset V \times \Omega$. Then,

$$(\mathcal{B}f)(x) - \frac{1}{(2\pi)^3} \int_{\mathbb{R}^3} B(x,\xi)\eta(x,\xi)\tilde{f}(\xi)e^{-i\xi\cdot x}\,d\xi \in C^\infty(V)\,, \tag{3.8}$$

where $\eta \in C^\infty(U \times \mathbb{R}^3)$, $\eta(x,\xi) = \eta(x,\xi/|\xi|)$ for $|\xi| \geq 1$, $\eta(x,\xi) \equiv 1$ on $V \times \Omega$ for $|\xi| \geq 1$, and supp $\eta \cap \mathrm{Crit}(C,\phi) = \varnothing$.

Proof. By construction no plane $\Pi(x,\xi)$, $(x,\xi) \in$ supp η, is tangent to C. Denote $\eta_c = 1 - \eta$, and represent the last integral in (2.19) as a sum of two functions

$$\begin{aligned} \Phi(s,x) &:= \int_{\mathbb{R}^3} \tilde{f}(\xi)\eta(x,\xi)e^{-i\xi\cdot y(s)}\delta'(\xi\cdot\beta(s,x))|\xi\cdot e(s,x)|\,d\xi\,, \\ \Phi_c(s,x) &:= \int_{\mathbb{R}^3} \tilde{f}(\xi)\eta_c(x,\xi)e^{-i\xi\cdot y(s)}\delta'(\xi\cdot\beta(s,x))|\xi\cdot e(s,x)|\,d\xi\,. \end{aligned} \tag{3.9}$$

Since $\beta \cdot e = 0$, $|\beta| = |e| = 1$, denote

$$F(p,q,r;s,x) := \tilde{f}(\xi)\eta_c(x,\xi)e^{-i\xi\cdot y(s)},\ \xi = \xi(p,q,r) = p\beta + qe + r(\beta\times e), \tag{3.10}$$

where $\beta = \beta(s,x)$, $e = e(s,x)$. Then,

$$\Phi_c(s,x) = -\int_{\mathbb{R}^2} F'_p(0,q,r;s,x)|q|\,dq\,dr\,. \tag{3.11}$$

By construction, $\tilde{f}(\xi)\eta_c(x,\xi)$, $x \in V$, is smooth and decays rapidly as $|\xi| \to \infty$. Hence, from (3.10) and (3.11), $\Phi_c \in C^\infty$ in a neighborhood of any $x \in V$, $s \in I(x)$, and subsequent integration with respect to s gives a $C^\infty(V)$ function. Following the steps (2.19)–(2.28), $\Phi(s,x)$ gives the same expression as in (2.28), but with $\eta(x,\xi)$ inserted in the integrand. These steps are now justified and no extra terms will appear, because $\xi\cdot\dot{y}(s)$ is bounded away from zero when $(x,\xi) \in$ supp η, $s \in I(x)$.

Performing the same splitting as in (3.9) for the second integral with respect to γ in (2.10), using the same argument as in the preceding paragraph, and combining similar terms, we finish the proof. □

Let us formulate additional notation, which will be used in the remainder of the article.

$$\begin{aligned} \Pi(s) &:= \left\{ y \in \mathbb{R}^3 :\ y = y(s) + t_1\dot{y}(s) + t_2\ddot{y}(s),\ t_{1,2} \in \mathbb{R} \right\}\,, \\ L(x,s) &:= \left\{ y \in \mathbb{R}^3 :\ y = y(s) + (x - y(s))t, t \in \mathbb{R} \right\}\,. \end{aligned} \tag{3.12}$$

Thus, $\Pi(s)$ is a plane through $y(s)$ and parallel to $\dot{y}(s)$, $\ddot{y}(s)$. $L(x,s)$ is a line through x and $y(s)$.

Theorem 4.

Let $f \in \mathcal{E}'(U)$. $\mathcal{B}f$ has non-local artifacts contained in the sets

$$\begin{aligned} E_1(f,C,\phi) &= \left\{(x,\xi) \in U \times \left(\mathbb{R}^3 \setminus 0\right) : (z,\xi) \in WF(f), \right. \\ &\qquad \left. z \in \Pi(s) = \Pi(x,\xi), s \in I(x)\right\}, \\ E_2(f,C,\phi) &= \left\{(x,\xi) \in U \times \left(\mathbb{R}^3 \setminus 0\right) : (z,\xi) \in WF(f), z \in L(x,s), \right. \\ &\qquad \left. \xi \cdot (x - y(s)) = \xi \cdot \dot{y}(s) = 0, s \in I(x)\right\}, \end{aligned} \tag{3.13}$$

that is

$$WF(\mathcal{B}f) \subset WF(f) \cup E_1(f,C,\phi) \cup E_2(f,C,\phi)\,. \tag{3.14}$$

Proof. By using partition of unity we can assume that I is an arbitrarily small neighborhood of some $s_0 \in I(x_0)$. Fix $x_0 \in U$ and denote $\xi_0 = (x_0 - y(s_0)) \times \dot{y}(s_0)$. It follows from (2.10) that the value of $\mathcal{B}f$ at x_0 depends only on values of f in a small neighborhood of $\Pi(x_0,\xi_0)$. Therefore, we can assume without loss of generality that supp f is contained sufficiently close to that plane.

Changing variables in (3.4): $v_1, v_2, s \to z = (z_1, z_2, z_3)$ according to $z = y(s) + v_1(x - y(s)) + v_2\dot{y}(s)$, we get

$$z'_{v_1} = x - y(s),\ z'_{v_2} = \dot{y}(s),\ z'_s = (1 - v_1)\dot{y}(s) + v_2\ddot{y}(s)\,. \tag{3.15}$$

The Jacobian of the transformation vanishes only if either $x \in \Pi(s)$ or $v_2 = 0$. Since A is C_0^∞ in v_1, v_2, s and C^∞ in x, this implies that $x_0 \in$ singsupp $(\mathcal{B}f)$ in only two cases:

Case 1. $x_0 \in \Pi(s_0)$ and $\Pi(s_0) \cap$ singsupp $f \neq \varnothing$, or

Case 2. $L(x_0,s_0) \cap$ singsupp $f \neq \varnothing$.

Therefore, if Case 2 holds, we can assume that f is supported in a small neighborhood of $L(x_0,s_0)$. Similar to Theorem 3, assume supp $f \subset V$ and $WF(f) \subset V \times \Omega$, where $V \times \Omega$ is a small conic neighborhood of some $(x',\xi'), \xi' \neq 0$. Here $x' \in \Pi(s_0)$ or $L(x_0,s_0)$ depending on the case. Suppose first $\xi_0 \notin \Omega$ and, shrinking $V \times \Omega$ if necessary, $(\overline{V \times \Omega}) \cap \mathrm{Crit}(C,\phi) = \varnothing$. By Theorem 3 we can assume $x_0 \notin V$. Representing f in terms of its Fourier transform in (3.4) we get

$$(\mathcal{B}f)(x) = \int_{\mathbb{R}^3} \tilde{f}(\xi) \int_I \int_{\mathbb{R}^2} \frac{A(s,x,v_1,v_2)}{(2\pi)^3 v_2^2} e^{-i\xi\cdot(y(s)+v_1(x-y(s))+v_2\dot{y}(s))}\, dv_1\, dv_2\, ds\, d\xi. \tag{3.16}$$

If x', x_0, and $y(s_0)$ are on one line, our assumptions imply that v_1 is separated from one and v_2 is close to zero. Considering the integral with respect to v_1 and s we see that it does not have a stationary point when $\xi \in \Omega$. Indeed, ξ would have to satisfy

$$\xi \cdot (\dot{y}(s)(1 - v_1) + v_2\ddot{y}(s)) = 0,\ \xi \cdot (x - y(s)) = 0\,. \tag{3.17}$$

Setting $s = s_0, x = x_0, v_2 = 0, v_1 \neq 1$ implies $\xi \cdot \dot{y}(s_0) = 0, \xi \cdot (x - y(s_0)) = 0$, that is $\xi \in \mathrm{Crit}(C,\phi)$. Since $\tilde{f}(\xi)$ decays rapidly outside Ω, $(\mathcal{B}f)(x)$ is C^∞ in a neighborhood of x_0.

If x', x_0, and $y(s_0)$ are not on one line, then, $v_2 \neq 0$ and a similar argument shows that the integral with respect to v_1, v_2, and s does not have a stationary point when $\xi \in \Omega$. Again, $(\mathcal{B}f)(x)$ is C^∞ near x_0.

Finally, if Ω is a conic neighborhood of the critical direction ξ_0, we multiply (3.16) by $g(x)\exp(i\lambda\nu \cdot x)$, where $g \in C_0^\infty(U)$ and $\nu \notin \Omega$, and integrate with respect to x first. This produces a C_0^∞ factor $\check{A}(s, v_1, v_2; \lambda\nu - v_1\xi)$ in the integrand. $\check{A}$ decays rapidly with respect to its last argument. Recall that v_1 varies over a compact set not containing zero. Since $\nu \notin \Omega$, $\tilde{f}(\xi)$ decays rapidly outside of Ω, and $1/v_2^2$ is a distribution of finite order, the standard argument implies that the entire integral decays rapidly as $\lambda \to \infty$.

Combining the considered cases with Theorem 3 we finish the proof. □

Combining Theorems 3 and 4 we conclude that outside $\mathrm{Crit}(C, \phi)$, $\mathcal{B}$ behaves just like an ordinary PDO with symbol $B(x, \xi)$ given by (2.12). This is stated more precisely in the following theorem.

Theorem 5.

Fix $(x_0, \xi_0) \in U \times (\mathbb{R}^3 \setminus 0)$, $(x_0, \xi_0) \notin \mathrm{Crit}(C, \phi)$. *Take any* $\eta_0 \in C^\infty(U \times \mathbb{R}^3)$, $\eta_0(x, \xi) = \eta_0(x, \xi/|\xi|)$ *for* $|\xi| \geq 1$, *such that* $\eta_0(x, \xi) \equiv 1$ *in a conic neighborhood of* (x_0, ξ_0) *for* $|\xi| \geq 1$, *and* $\mathrm{supp}\ \eta_0 \cap \mathrm{Crit}(C, \phi) = \varnothing$. *Then,*

$$(\mathcal{B}f)(x) - \frac{1}{(2\pi)^3}\int_{\mathbb{R}^3} B(x, \xi)\eta_0(x, \xi)\tilde{f}(\xi)e^{-i\xi\cdot x}\, d\xi \in C^\infty \tag{3.18}$$

microlocally near (x_0, ξ_0) *for all* $f \in \mathcal{E}'(U)$.

We recall for convenience that a distribution f is C^∞ microlocally near $(x_0, \xi_0) \in \mathbb{R}^n \times (\mathbb{R}^n \setminus 0)$ if for some $\varphi \in C_0^\infty(\mathbb{R}^n)$ which equals one in a neighborhood of x_0, $\widehat{(\varphi f)}(\xi)$ decays rapidly in a conic neighborhood of ξ_0 (cf. [20], p. 58–59). The difference between Theorems 3 and 5 is that in the former $WF(f) \subset V \times \Omega$, and in the latter this assumption is dropped.

Proof. By using microlocal partition of unity write $f = f_1 + f_2$, where $\mathrm{supp}\ f_{1,2} \subset U$, $WF(f_1) \cap \mathrm{Crit}(C, \phi) = \varnothing$, and $WF(f_2)$ is contained in a sufficiently small conic neighborhood of $\mathrm{Crit}(C, \phi)$. In particular, $(x_0, \xi_0) \notin WF(f_2)$. Covering $WF(f_1)$ by sufficiently small open conic sets $V_j \times \Omega_j$ which do not intersect $\mathrm{Crit}(C, \phi)$ and using the corresponding partition of unity, find distributions f_{1j} which satisfy:

$$f_1 = \sum_j f_{1j},\ \mathrm{supp}\ f_{1j} \subset U,\ WF(f_{1j}) \subset V_j \times \Omega_j\ . \tag{3.19}$$

By construction and Theorem 4 all the sets $E_{1,2}(f_{1j}, C, \phi)$ are empty. Using Theorem 4 for distributions f_{1j} with $x_0 \notin V_j$, and Theorem 3—for f_{1j} with $x_0 \in V_j$, we conclude

$$(\mathcal{B}f_1)(x) - \frac{1}{(2\pi)^3}\sum_{j:x_0\in V_j}\int_{\mathbb{R}^3} B(x, \xi)\eta_{1j}(x, \xi)\tilde{f}_{1j}(\xi)e^{-i\xi\cdot x}\, d\xi \in C^\infty \tag{3.20}$$

in a neighborhood of x_0, where η_{1j} have the properties stated in Theorem 3. Since all $B\eta_{1j}$ and $B\eta_0$ are conventional amplitudes, (3.20) implies

$$\begin{aligned}(\mathcal{B}f_1)(x) - \frac{1}{(2\pi)^3}\int_{\mathbb{R}^3} B(x, \xi)\eta_0(x, \xi)\tilde{f}_1(\xi)e^{-i\xi\cdot x}\, d\xi \in C^\infty\ ,\\ (\mathcal{B}f_1)(x) - \frac{1}{(2\pi)^3}\int_{\mathbb{R}^3} B(x, \xi)\eta_0(x, \xi)\tilde{f}(\xi)e^{-i\xi\cdot x}\, d\xi \in C^\infty\ ,\end{aligned} \tag{3.21}$$

near x_0. From (3.13), $E_{1,2}(f, C, \phi) \subset \text{Crit}(C, \phi)$ for any $f \in \mathcal{E}'(U)$. Therefore, $WF(\mathcal{B}f_2) \subset \text{Crit}(C, \phi) \cup WF(f_2)$. By construction, $(x_0, \xi_0) \notin \text{Crit}(C, \phi) \cup WF(f_2)$, and the assertion of the theorem follows immediately from (3.21). □

4. Practical Implementation and Numerical Experiments

In this section we will discuss an efficient algorithm for computing $\mathcal{B}f$. Denoting

$$e(s, \beta) := \frac{[\beta \times \dot{y}(s)] \times \beta}{|[\beta \times \dot{y}(s)] \times \beta|}, \beta \in S^2 , \tag{4.1}$$

rewrite (2.10) as follows:

$$\mathcal{B}f(x) := -\frac{1}{2\pi^2} \int_I \left\{ \psi_1(s, x)\Psi_1(s, \beta(s, x)) - \psi_2(s, x)\Psi_2(s, \beta(s, x)) \right\} ds , \tag{4.2}$$

$$\Psi_1(s, \beta) = \int_0^{2\pi} D_f(y(s), \cos\gamma\beta + \sin\gamma e(s, \beta)) \frac{\cos\gamma}{\sin^2\gamma} d\gamma , \tag{4.3}$$

$$\Psi_2(s, \beta) = \int_0^{2\pi} D_f(y(s), \cos\gamma\beta + \sin\gamma e(s, \beta)) \frac{1}{\sin\gamma} d\gamma . \tag{4.4}$$

Let ω be the polar angle in the plane through $y(s)$ and perpendicular to $\dot{y}(s)$, and $\alpha(\omega)$ be the corresponding unit vector. Fix ω, $0 \le \omega < 2\pi$, and let $\Pi(\omega)$ denote the plane spanned by $\dot{y}(s)$ and $\alpha(\omega)$. Here, for convenience, we think of vectors $\dot{y}(s)$, $\alpha(\omega)$, and β as attached to $y(s)$. Fix any $\beta \in \Pi(\omega)$. By construction, vectors $\cos\gamma\beta + \sin\gamma e(s, \beta)$, $0 \le \gamma < 2\pi$, belong to the same plane $\Pi(\omega)$. Let θ be the polar angle in that plane. Since $e \cdot \beta = 0$, $e \cdot e = 1$, we can write (with abuse of notation):

$$\beta = (\cos\theta, \sin\theta), \ e = (-\sin\theta, \cos\theta), \ \beta, e \in \Pi(\omega) . \tag{4.5}$$

Therefore,

$$\begin{aligned} \Psi_1(s, \beta) &= \int_0^{2\pi} D_f(y(s), (\cos(\theta + \gamma), \sin(\theta + \gamma))) \frac{\cos\gamma}{\sin^2\gamma} d\gamma , \\ \Psi_2(s, \beta) &= \int_0^{2\pi} D_f(y(s), (\cos(\theta + \gamma), \sin(\theta + \gamma))) \frac{1}{\sin\gamma} d\gamma, \ \beta \in \Pi(\omega) . \end{aligned} \tag{4.6}$$

Equations (4.6) are of convolution type. Therefore, one application of Fast Fourier Transform (FFT) to the integrals in (4.6) gives values of $\Psi_{1,2}(s, \beta)$ for all $\beta \in \Pi(\omega)$ at once. Equations (4.2) and (4.6) imply that the resulting algorithm is of the filtered-backprojection type. First, one computes shift-invariant filtering of cone beam projections according to (4.6) for all required ω, and the second step is backprojection (4.2). Obviously, every projection is processed as soon as it has been acquired and is never used later.

Consider now two numerical experiments. Parameters of the data collection protocol are the same in both of them and are given in Table 1.1.

In Figure 2 we show the results of reconstructing the 3-D low contrast Shepp phantom (see Table 1 in [8]). In the left panel we see a vertical slice through the reconstructed image at $x_1 = -0.25$, and in the right panel—the graphs of exact (dashed line) and computed

TABLE 1.1

Parameters of the Data Collection Protocol	
R (radius of the spiral)	3
h (pitch of the spiral)	0.5
axial span of the detector array	0.96
transverse span of the detector array	4.26
number of detector rows	50
number of detectors per row	500
number of source positions per one turn of the spiral	500

(solid line) values of f along a vertical line $x_1 = -0.25, x_2 = 0$. We used the grey scale window [1.01, 1.03] to make low-contrast features visible. Axial span of the section of spiral used in this experiment was $|y_3(s)| \leq 1.5$, with the phantom concentrated in the region $|x_3| \leq 0.92$. Note that both in this and the second experiment we did not attempt to find the shortest section of the spiral compatible with the algorithm.

In Figure 3 we see the results of reconstructing the disk phantom, which consists of six identical flattened ellipsoids (lengths of half-axes: 0.75, 0.75, and 0.04, distance between centers of neighboring ellipsoids: 0.16). In the left panel we see a vertical slice through the reconstructed image at $x_1 = 0$, and in the right panel—the graphs of exact (dashed line) and computed (solid line) values of f along a vertical line $x_1 = 0, x_2 = 0$. Axial span of the section of spiral used in this experiment was $|y_3(s)| \leq 1.0$, with the phantom concentrated in the region $|x_3| \leq 0.44$.

As one can conclude from the discussion following Theorem 1, relatively strong artifacts might be expected if $WF(f)$ has a significant component near the axial direction, and minor artifacts—otherwise. This conclusion is confirmed by comparing the density plots in Figures 2 and 3. The artifacts in Figure 3 are much stronger than those in Figure 2, because in the former case, loosely speaking, most of the energy of $WF(f)$ is concentrated near the axial direction. These artifacts are typical for all FBP-type algorithms (see e. g., [14, 10]).

If we look carefully at the density plot in Figure 3, it will become noticeable that the artifacts in $\mathcal{B}f$ are of two types. This is in agreement with Theorem 4. Artifacts of the first type are straight lines that are almost horizontal and tangent to the ellipsoids. These lines are intersections of the planes in $E_1(f, C, \phi)$ with $x_1 = 0$. Artifacts of the second type are less regular. They arise in part because of discretization errors, and in part they correspond to intersections of the lines in $E_2(f, C, \phi)$ with the plane $x_1 = 0$.

5. Regularization of Integrals in (2.19)

Without loss of generality we can assume that $y(s)$ is at the origin, $\beta(s, x)$ is along the first coordinate axis, and $e(s, x)$ is along the second axis. For convenience, we omit the dependence of f and D_f on the third spatial variable. The regularized version of the first integral with respect to γ in (2.10) is

$$\lim_{\epsilon \to 0} \left\{ \int_{-\pi+a}^{-\epsilon} + \int_{\epsilon}^{\pi-a} \right\} \frac{(\partial/\partial\gamma) D_f(0, (\cos\gamma, \sin\gamma))}{\sin\gamma} \, d\gamma \,, \tag{5.1}$$

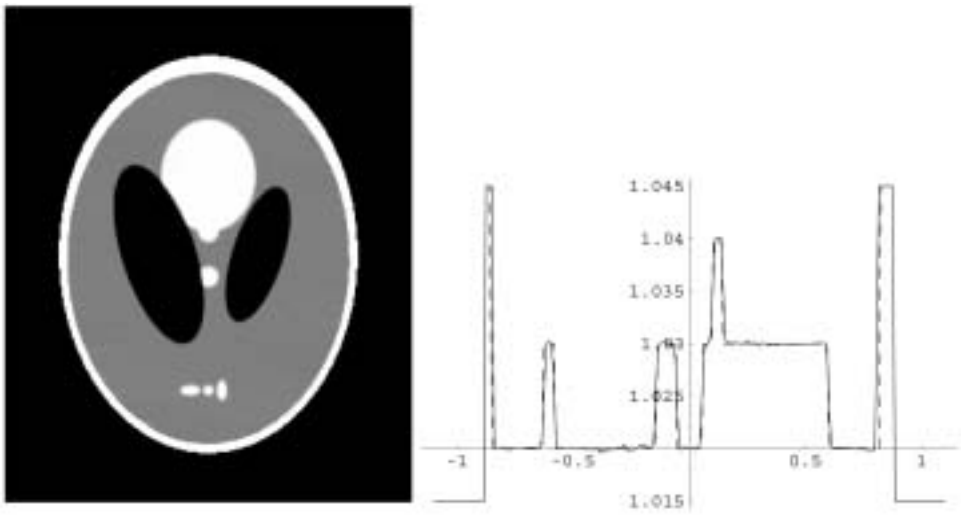

FIGURE 2 Reconstruction of the 3-D Shepp phantom.

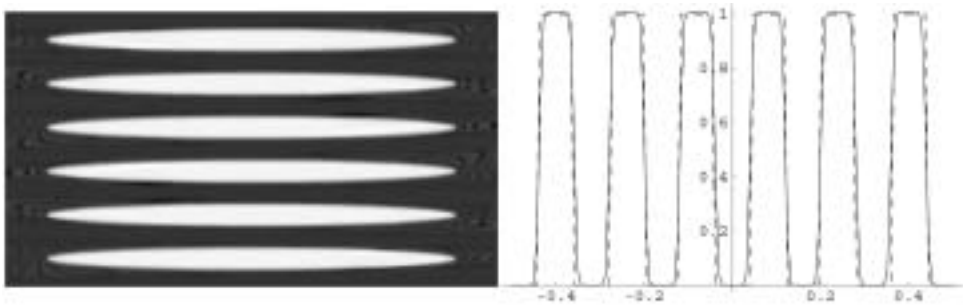

FIGURE 3 Reconstruction of the disk phantom.

where we have used that supp f belongs to the wedge $|\gamma| \le \pi - a$ for some $a > 0$. Here γ is the polar angle in the x_1-x_2 plane. Substitution of the definition of D_f gives

$$\begin{aligned}\lim_{\epsilon\to 0}\left\{\int_{-\pi+a}^{-\epsilon}+\int_{\epsilon}^{\pi-a}\right\}\frac{1}{\sin\gamma}\int_0^\infty\Big[f_1'(t\cos\gamma,t\sin\gamma)(-t\sin\gamma)\\ +f_2'(t\cos\gamma,t\sin\gamma)t\cos\gamma\Big]\,dt\,d\gamma \qquad (5.2)\\ =\lim_{\epsilon\to 0}\left[-\int_{D_\epsilon}f_1'(x_1,x_2)dx_1dx_2+\int_{D_\epsilon}f_2'(x_1,x_2)\frac{x_1}{x_2}\,dx_1\,dx_2\right],\end{aligned}$$

where $f'_{1,2} := \partial f/\partial x_{1,2}$ and D_ϵ is the exterior of the wedge $|\gamma| \le \epsilon$. It is obvious now that the limit of the first integral equals zero, and the second integral can be written exactly as in the last line of (2.19). The second integral in (2.10) can be regularized in a similar fashion.

6. End of the Proof of Theorem 1

Throughout this section $x \in U$ is fixed. Fix any $\eta \in C^\infty(\mathbb{R})$, $\eta(t) = 0$, $|t| \le 1$, and $\eta(t) = 1$, $|t| \ge 2$. As easily seen, the last integral in (2.19) can be replaced by

$$\frac{-i}{4\pi} \lim_{\epsilon \to 0^+} \int_{\mathbb{R}^3} \tilde{f}(\xi) e^{-i\xi \cdot y(s)} \delta'(\xi \cdot \beta(s,x)) \eta(\xi \cdot e(s,x)/\epsilon) |\xi \cdot e(s,x)| \, d\xi \, . \tag{6.1}$$

Consider now the step from (2.19) to (2.20) in more detail. Upon omitting irrelevant constants, we have after substituting (6.1) into the first integral in (2.10).

$$\int_I \psi_1(s,x) \left\{ \lim_{\epsilon \to 0^+} \int_{\mathbb{R}^3} \tilde{f}(\xi) e^{-i\xi \cdot y(s)} \delta'(\xi \cdot \beta(s,x)) \eta\left(\frac{\xi \cdot e(s,x)}{\epsilon}\right) |\xi \cdot e(s,x)| \, d\xi \right\} ds. \tag{6.2}$$

Let $A_\epsilon(s)$ be the function defined by the integral in (6.1). Since $\beta \cdot e = 0$ and $\tilde{f}(\xi) \in \mathcal{S}(\mathbb{R}^3)$, we conclude that $A_\epsilon(s)$, $\epsilon \to 0^+$, is a bounded sequence of C^∞ functions that converges to a limit. This limit, of course, is the function defined by the same integral with η removed. Thus, by Lebesgue's Dominated Convergence Theorem (LDCT), we can move $\lim_{\epsilon \to 0^+}$ outside. Suppose now $\epsilon > 0$ is fixed, and let $\delta'_{\epsilon_1} \in C_0^\infty(\mathbb{R})$, $\epsilon_1 \to 0^+$, be a sequence converging to δ' in $\mathcal{D}'(\mathbb{R})$. Replacing δ' with δ'_{ϵ_1}, inserting $\lim_{\epsilon_1 \to 0^+}$, and, then, changing the order of integration, we get:

$$\lim_{\epsilon_1 \to 0^+} \int_{\mathbb{R}^3} \tilde{f}(\xi) \left\{ \int_I \psi(s,x) e^{-i\xi \cdot y(s)} \delta'_{\epsilon_1}(\xi \cdot \beta(s,x)) \eta\left(\frac{\xi \cdot e(s,x)}{\epsilon}\right) |\xi \cdot e(s,x)| ds \right\} d\xi. \tag{6.3}$$

Similarly to (2.20), we can change variables $s \to v = \xi \cdot \beta(s,x)$. Now the problem that $v'_s = \xi \cdot \beta'_s(s,x) = 0$ for some ξ is no longer a concern, because [cf. (2.25)]

$$\beta'_s(s,x) = \left(\frac{x - y(s)}{|x - y(s)|}\right)' = -\frac{\dot{y}(s) - (\beta \cdot \dot{y}(s))\beta}{|x - y(s)|} = -\frac{e(s,x)}{b|x - y(s)|} \, , \tag{6.4}$$

and $\xi \cdot \beta'_s(s,x) = 0$ implies $\xi \cdot e(s,x) = 0$, $\eta(\xi \cdot e(s,x)/\epsilon) = 0$. Just as in (2.20), the term v'_s will appear in the denominator. Since $\epsilon > 0$ is fixed, $v'_s = \xi \cdot \beta'_s(s,x)$ is bounded away from zero on supp $\eta(\xi \cdot e(s,x)/\epsilon)$. Therefore, we can use LDCT to bring $\lim_{\epsilon_1 \to 0^+}$ inside the integral with respect to ξ. This gives

$$\int_{\mathbb{R}^3} \tilde{f}(\xi) \left\{ \int_I \psi(s,x) e^{-i\xi \cdot y(s)} \delta'(\xi \cdot \beta(s,x)) \eta\left(\frac{\xi \cdot e(s,x)}{\epsilon}\right) |\xi \cdot e(s,x)| \, ds \right\} d\xi \, . \tag{6.5}$$

In view of (2.22), the analog of the last equation in (2.20) becomes

$$\left[-i \sum_j \phi(s_j,x) \eta(\xi \cdot e(s_j,x)/\epsilon) + \sum_j \frac{1}{t'_s} \frac{\partial}{\partial s} \{\phi A \eta\} \Big|_{s=s_j} \right] e^{-i\xi \cdot x} \, . \tag{6.6}$$

Combining (6.6) with an analogous expression for $I_2(x)$ [which contains an expression, that can be put in the form $-\sum_j (1/t'_s)\eta \partial(\phi A)/\partial s\big|_{s=s_j}$, cf. (2.23), (2.27), (2.30), and (2.31)], we get

$$\begin{aligned} (\mathcal{B}f)(x) = \frac{1}{(2\pi)^3} \lim_{\epsilon \to 0^+} \int_{\mathbb{R}^3} \tilde{f}(\xi) e^{-i\xi \cdot x} \sum_j \phi(s_j,x) \\ \times \left[\eta\left(\frac{\xi \cdot e(s_j,x)}{\epsilon}\right) + \eta'\left(\frac{\xi \cdot e(s_j,x)}{\epsilon}\right) \frac{i(\xi \cdot e'_s(s_j,x))}{\epsilon(\xi \cdot \dot{y}(s_j))} \right] d\xi \, . \end{aligned} \tag{6.7}$$

Since the set $\{\xi \in \mathbb{R}^3 : \xi \cdot \dot{y}(s_j) = 0\}$ has Lebesgue measure zero in $\mathbb{R}^3$, LDCT can obviously be used for the integral involving the first term in brackets in (6.7), and we obtain the first term in (2.11). Consider now the second term. Similarly to (2.20), we establish using (2.31):

$$\begin{aligned}
&\int_{\mathbb{R}^3} \tilde{f}(\xi) e^{-i\xi\cdot x} \sum_j \phi(s_j, x) \eta'\left(\frac{\xi \cdot e(s_j, x)}{\epsilon}\right) \frac{i\left(\xi \cdot e_s'(s_j, x)\right)}{\epsilon(\xi \cdot \dot{y}(s_j))}\, d\xi \\
&\quad = \int_I \frac{\phi(s, x)}{|x - y(s)|} \int_{\mathbb{R}^3} \tilde{f}(\xi) e^{-i\xi\cdot y(s)} \eta'\left(\frac{\xi \cdot e(s, x)}{\epsilon}\right) \frac{i\left(\xi \cdot e_s'(s, x)\right)}{\epsilon} \\
&\qquad \times \delta(\xi \cdot \beta(s, x)) \operatorname{sgn}(\xi \cdot e(s, x))\, d\xi\, ds\ .
\end{aligned} \tag{6.8}$$

As in the proof of Theorem 3, write $\xi = p\beta + qe + r(\beta \times e)$, and the integral with respect to ξ becomes

$$\int_{\mathbb{R}^2} F(0, q, r) \eta'(q/\epsilon) \frac{ir\left([\beta \times e] \cdot e_s'\right)}{\epsilon} \operatorname{sgn}(q)\, dq\, dr\ , \tag{6.9}$$

$$F(p, q, r) := \tilde{f}(\xi) e^{-i\xi\cdot x},\ \xi = \xi(p, q, r)\ . \tag{6.10}$$

Here we have also used that $e \cdot e_s' = 0$ and $\xi \cdot y(s) = \xi \cdot x$ when $p = 0$. Consider the integral with respect to q:

$$\begin{aligned}
&\int_{\mathbb{R}} F(0, q, r) \eta'(q/\epsilon) \frac{1}{\epsilon} \operatorname{sgn}(q)\, dq \\
&\quad = -\int_0^\infty F_q'(0, q, r) \eta(q/\epsilon)\, dq \\
&\qquad + \int_{-\infty}^0 F_q'(0, q, r) \eta(q/\epsilon)\, dq \to\ 2F(0, 0, r),\ \epsilon \to 0\ ,
\end{aligned} \tag{6.11}$$

where we have used that $\eta(0) = 0$ and $F(0, \pm\infty, r) = 0$. Setting $q = 0$ in (6.10) and using (6.11) we find the limit of (6.8) as $\epsilon \to 0^+$:

$$2i \int_I \frac{\phi(s, x)}{|x - y(s)|} \int_{\mathbb{R}} \tilde{f}(\xi) (\xi \cdot e_s') e^{-i\xi\cdot x}\, dr\, ds,\ \xi = r[\beta \times e]\ , \tag{6.12}$$

which, after taking care of constants, gives the second term in (2.11).

References

[1] Danielsson, P.E., et al. (1997). Towards exact reconstruction for helical cone-beam scanning of long objects. A new detector arrangement and a new completeness condition, *Proc. 1997 Meeting on Fully 3D Image Reconstruction in Radiology and Nuclear Medicine*, (Pittsburgh), Townsend, D.W. and Kinahan, P.E., Eds., 141–144.

[2] Defrise, M., Noo, F., and Kudo, H. (2000). A solution to the long-object problem in helical cone-beam tomography, *Physics in Medicine and Biology*, **45**, 623–643.

[3] Faridani, A. (1997). Results, old and new, in computed tomography, *Inverse Problems in Wave Propagation, The IMA Volumes in Mathematics and its Applications*, Chavent, G., Papanicolaou, G., Sacks, P., and Symes, W., Eds., vol. 90, Springer-Verlag, New York, 167–193.

[4] Feldkamp, L.A., Davis, L.C., and Kress, J.W. (1984). Practical cone-beam algorithm, *J. Opt. Soc. Am.*, **1**, 612–619.

[5] Greenleaf, A. and Uhlmann, G. (1989). Nonlocal inversion formulas for the X-ray transform, *Duke Mathematical J.*, **58**, 205–240.

[6] Katsevich, A. (1999). Cone beam local tomography, *SIAM J. on Applied Mathematics*, 2224–2246.

[7] Katsevich, A. (2000). On quasi-local inversion of spiral CT data, *Applicable Analysis*, **23**, 271–297.

[8] Kudo, H., Miyagi, N., and Saito, T. (1998). A new approach to exact cone-beam reconstruction without Radon transform, IEEE Nuclear Science Symposium Conference Record, *IEEE*, 1636–1643.

[9] Kudo, H., Noo, F., and Defrise, M. (1998). Cone-beam filtered-backprojection algorithm for truncated helical data, *Phys. Med. Biol.*, **43**, 2885–2909.

[10] Kudo, H., Park, S., Noo, F., and Defrise, M. (1999). Performance of quasi-exact cone-beam filtered backprojection algorithm for axially truncated helical data, *IEEE Trans. Nucl. Sci.*, **46**, 608–617.

[11] Kudo, H. and Saito, T. (1997). An extended cone-beam reconstruction using Radon transform, 1996 IEEE Med. Imag. Conf. Record, *IEEE*, 1693–1697.

[12] Lan, I.-R. (1999). On an operator associated to a restricted x-ray transform, Ph.D. thesis, Oregon State University.

[13] Louis, A.K. and Maass, P. (1993). Contour reconstruction in 3-D X-ray CT, *IEEE Transactions on Medical Imaging*, **12**, 764–769.

[14] Noo, F., Kudo, H., and Defrise, M. (1998). Approximate short-scan filtered-backprojection for helical CB reconstruction, Conf. Rec. 1998 IEEE Nuclear Science Symposium, (Toronto, Ont., Canada), vol. 3, *IEEE*, Piscataway, NJ, 2073–2077.

[15] Quinto, E.T. (1993). Singularities of the X-ray transform and limited data tomography in $\mathbb{R}^2$ and $\mathbb{R}^3$, *SIAM J. of Mathematical Analysis*, **24**, 1215–1225.

[16] Ramm, A. and Katsevich, A. (1996). *The Radon Transform and Local Tomography*, CRC Press, Boca Raton, FL.

[17] Tam, K.C. (1995). Method and apparatus for converting cone beam x-ray projection data to planar integral and reconstructing a three-dimensional computerized tomography (CT) image of an object, US. Patent 5,257,183, October.

[18] Tam, K.C. (1997). Cone-beam imaging of a section of a long object with a short detector, Information processing in medical imaging, Duncan, J.S. and Gindi, G.R., Eds., *Lecture Notes in Computer Science*, vol. 1230, Springer, Berlin, 525–530.

[19] Turbell, H. and Danielsson, P.-E. (2000). Helical cone beam tomography, *Int. J. of Imaging Syst. and Technology*, **11**, 91–100.

[20] Treves, F. (1980). *Introduction to Pseudodifferential and Fourier Integral Operators. Volume 1: Pseudodifferential Operators*, The University Series in Mathematics, Plenum, New York.

Received October 4, 2000

Department of Mathematics, University of Central Florida, Orlando, FL 32816-1364
e-mail: akatsevi@pegasus.cc.ucf.edu